Online Supplemental Material for

J. Gen. Physiol. Vol. 117 No. 4 p. 329, Grabe and Oster

Detailed Calculations and Discussion

Michael Grabe and George Oster

V-ATPase Model

We have constructed a mechanochemical model for the V-ATPase that predicts proton pumping rates over a wide range of environmental conditions. We have used this model to determine the acidification of organelles. The conventional paradigm for active transmembrane ion transport is the "alternating access" mechanism: ions are bound tightly on the low concentration side of the membrane and a conformational change exposes them to the high concentration side and weakens their binding affinity so that they dissociate. The pump then resets its conformation to repeat the cycle (Eisenberg and Hill, 1985; Alberts et al., 1994). The energy to drive the cycle is supplied by nucleotide hydrolysis or an ion gradient. The Na-K-ATPase conforms to this traditional view of alternating access (see below); however, the conformational change in the V-ATPase is a simple rotation. In our computations here, we assume that the V-ATPase is working under normal operating conditions and that ATP concentrations are sufficiently high that hydrolysis is not rate limiting.

By analogy with the F-ATPases, the V-ATPase structure is conventionally divided into a counter-rotating "stator" and "rotor" (Boekema et al., 1997; Finbow and Harrison, 1997; Forgac, 2000). Hydrolysis of ATP in the V_1-soluble headpiece provides the torque that rotates the membrane-bound section V_o. Two models have been suggested for the rotor–stator assemblies: a two-channel model and a one-channel model (Vik and Antonio, 1994; Junge et al., 1997; Elston et al., 1998; Grabe et al., 2000). They differ in the path that the protons take through the enzyme and in the degree to which protons bound to the rotor section communicate with the cytoplasm. There is significant debate about the true structure of the channel in the V- and F-ATPase enzymes. We have shown that both channels behave similarly within the context of our mechanochemical model (Dimroth et al., 1999; Grabe et al., 2000). More recently, experiments on sodium V-ATPases strongly support the one channel model (Murata et al., 2000). There-

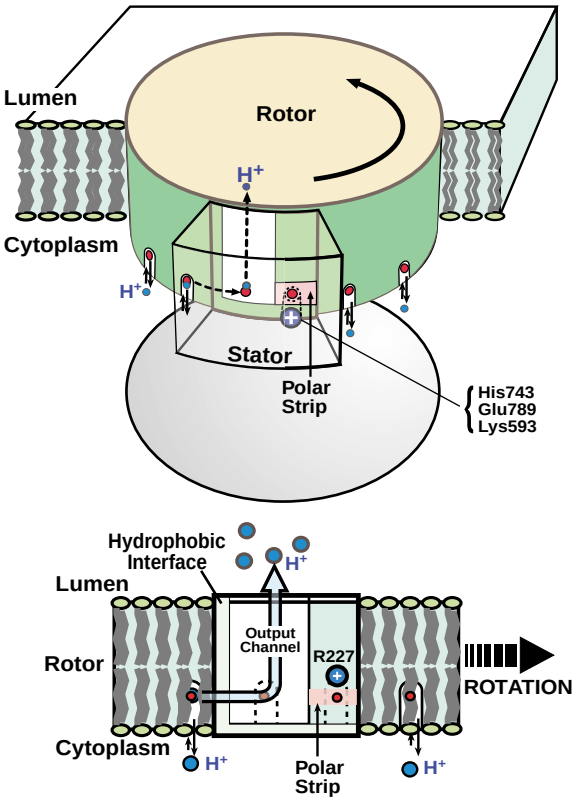

Figure S1. Perspective and face-on views of the rotor–stator assembly showing the paths protons follow in moving from the cytoplasm (bottom) into the lumen (top). Torque supplied by V_1 from ATP hydrolysis turns the rotor to the right. A single half channel penetrates the stator to the level of the rotor sites. A horizontal polar strip connects the right side of the channel and the cytoplasm to allow the passage of an unprotonated site, but protons are blocked from leaking by the stator charge. All other parts of the rotor–stator interface are hydrophobic. Cytoplasmic protons on the left bind to a rotor site, largely neutralizing it. Rotation carries the protonated site across the hydrophobic interface where the site enters the output (acidic) channel (from the left). The stator charges force the site to relinquish its proton into the lumen. The unprotonated site exits the interface to the right and is again in equilibrium with the cytoplasmic reservoir. Note that the sizes of the rotor and stator are such that two rotor sites cannot fit in the rotor–stator interface at once.

J. Gen. Physiol. © The Rockefeller University Press • 0022-1295
Volume 117 April 2001
http://www.jgp.org/cgi/content/full/117/4/329/DC1

fore, in Fig. S1 we present the putative structure for the one-channel model that was used to compute the V-ATPase performance surface in Fig. 2 A of the text.

The structure in Fig. S1 must possess a few key properties to be a physically viable model. The interface between rotor and stator must present a hydrophobic barrier to prevent proton leakage between the reservoirs. When not in the stator interface, the six rotor acidic sites exchange protons with the cytoplasm. Finally, the output (acidic) channel extends into the stator to the level of the rotor proton binding sites to allow exchange with the lumen.

The one-channel proton pump model works according to the following sequence of events (shown in Fig. S2 A). Rotor sites are in equilibrium with the basic reservoir. Until a rotor site is protonated, the torque generated by V_1 cannot force it over the hydrophobic barrier. However, once neutralized by protonation, the torque from V_1 drives the site across the barrier into the stator output channel. A protonated site that rotates out of the channel into the polar strip interacts electrostatically with the stator charge, reducing its pK_a and forcing it to relinquish its proton to the acidic reservoir. Further rotation carries the rotor site out of the stator interface, where it quickly equilibrates with the basic reservoir. The full mathematical formulation is contained in the original paper (Grabe et al., 2000).

The pumping cycle in Fig. S2 A does not always culminate in the proton exiting through the output channel. Rather, the protonated site "slips" past the stator charge and reequilibrates with the input reservoir. Fig. S2 B out-

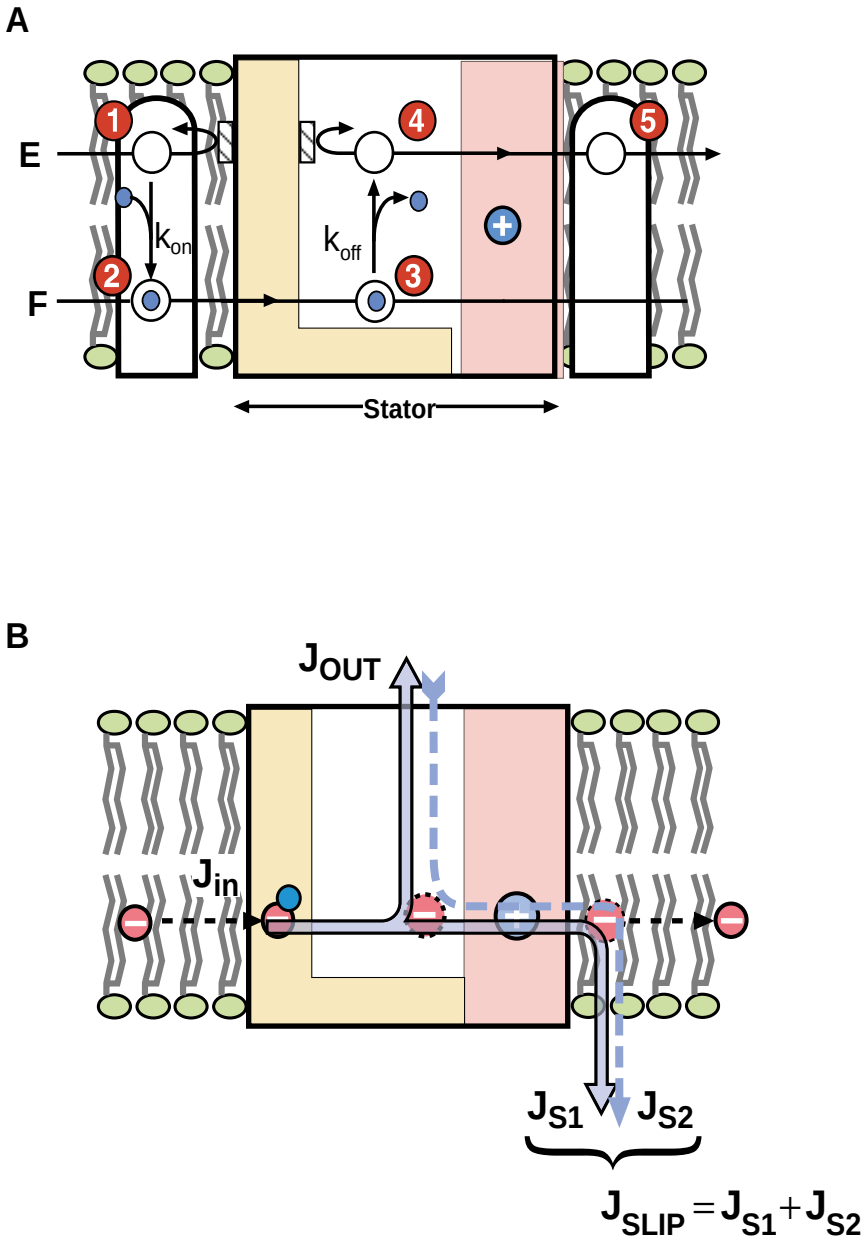

FIGURE S2. Mechanistic description of a typical pumping event and slip. (A) A typical sequence of events following a site as it passes through the rotor–stator interface. An empty site in the basic channel is reflected by the dielectric boundary until a proton binds, neutralizing the site (1 → 2). The V_1 motor rotates a protonated site out of the membrane, across the hydrophobic interface, and into the acidic channel (2 → 3). In the channel, the site has a high probability of staying protonated since k_{on} is large. However, when the protonated site rotates close to the stator charge, the rotor site pK_a decreases so that k_{off} increases until the proton is relinquished to the acidic reservoir (3 → 4). The empty site is then driven through the hydrophilic strip, past the stator charge, and into the basic reservoir (4 → 5). The torque from V_1 can then rotate the site through an entire revolution back to position (1) where the cycle repeats. (B) The possible pathways for protons passing through the stator. A fraction of the protons that rotate into the output channel slip past the stator charge and dissociate back into the basic reservoir. The proton flux (J_{IN}) traverses the hydrophobic interface from the left. A fraction (J_{OUT}) dissociates into the output channel, and a fraction (J_{S1}) slips past the stator charge and leaves the input channel; thus $J_{S1} = J_{IN} - J_{OUT}$. Actually, a site traversing the output channel will bind and dissociate a proton $\sim 10^4$–$10^5\times$, so the proton that slips back into the basic reservoir is unlikely to be the same one that initially entered on the rotor site (Grabe et al., 2000). Additionally, the back and forth diffusive motion of the rotor may shuttle protons from the output channel to the basic reservoir, creating a second contribution to the slip flux (J_{S2}). Thus, the total slip flux is $J_{SLIP} = J_{S1} + J_{S2}$. This second component of the slip flux is only important when the V_1 motor is nearly at stall; i.e., when the rotation rate of V_o is small.

lines various slip mechanisms. Slip can have a profound influence upon acidification since it limits the pH that a vesicle can attain. As the pmf across the membrane increases, the enzyme is more prone to slip. The degree of slip can only be determined experimentally from measuring ATP hydrolysis rates and proton pumping. The surface in Fig. S2 A is partially calibrated from patch-clamp experiments and largely free of slip over the range of plotted pmf's. Excellent reviews of this enzyme can be found in the February special edition of the *J. Bioenerg. Biomembr.* (2000).

The "Gear Change" Model for Hyperacidification

It is generally accepted that the V_1 subunit has three ATP hydrolyzing sites, while the V_o rotor has six proton binding sites on each of its proteolipid subunits (c, c′, and c″) that span the lipid bilayer. Under optimal conditions (i.e., no slip), every rotation of the enzyme transports six protons at the expense of three ATP's, corresponding to a coupling ratio of two. If the six proton binding sites have different pK_a's (for instance, three with low and three with high values), exposure to a very acidic lumenal environment would permanently titrate the high pK_a rotor sites. Then the number of active rotor sites would be reduced from six to three, thus decreasing the coupling ratio from two to one. With this coupling ratio, the energy of each ATP would transport one proton, and the maximum achievable pH gradient would double from 4.5 to 9. This may help account for the phenomenon of very acidic organelles. We have revisited the V-ATPase model above, assuming that the six proton binding sites are not equivalent. The sites are assumed to alternate between tightly binding, $pK_a \sim 7.3$, and weakly binding, $pK_a \sim 3.8$. We also assume that the tightly binding sites hold the proton much closer to the proton-accepting amino acid, creating a much smaller dipole electric field. The existence of more than one proteolipid subunit in the V-ATPase could explain this heterogeneity in proton binding sites. Although all three subunits (c, c′, and c″) are homologous, subtle differences in their proton binding carboxyl groups could account for the variations in proton binding affinities (Forgac, 1999).

In Fig. S3, the proton flux is plotted as a function of lumenal pH. The list of simulation parameters are given in Table SI. At modest lumenal pH values, pH ∼ 6–7, all sites participate in proton transport; however, as lumenal pH drops (pH ∼ 3.5–6), the high pK_a sites no longer deliver protons to the lumen. On average, these sites do no work against the pH gradient, thereby enabling the low pK_a sites to use a larger fraction of the energy of ATP hydrolysis and continue pumping protons. This proposed ability of the V-ATPase to sense and adjust to the absolute pH of the lumen is theoretically interesting. In more alkaline organelles, the V-ATPase works far from thermodynamic stall, where all six proton binding sites would participate in pumping in order to counter the high leak rate of protons. However, in the very acidic organelles, where proton permeabilities are likely to be small, the overall rate of proton pumping should be less important than the size of the pH gradient the enzyme can create. Therefore, as an organelle acidifies, the loss of some of the proton transporting sites is more than made up for by the enzyme's ability to continue working to produce a low lumenal pH.

These calculations are carried out in program files: v_pump.m (main program); cal_2.m; vel_a.m; v_param.m; barrier.m; delc_cf.m; pot.m; pot2.m.

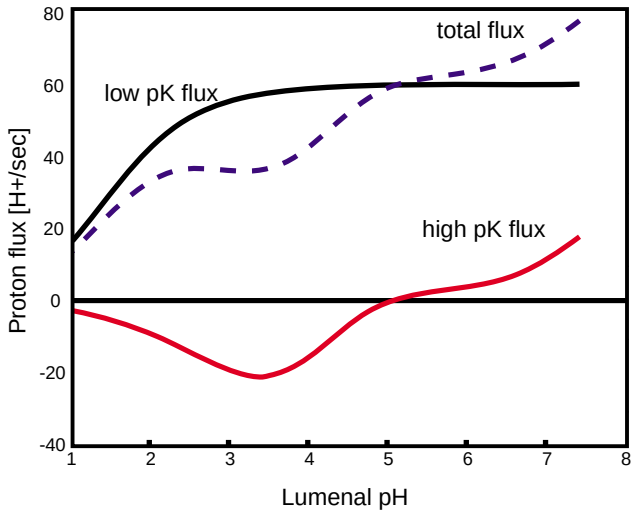

FIGURE S3. The proton flux of a single V-ATPase in the absence of membrane potential is plotted as a function of lumenal pH. It is generally accepted that the rotor subunit of the V-ATPase is composed of six proton binding sites. Here we explore the possibility that these sites have alternating high and low pK_a's. At high pH values, all sites participate in proton transport from the cytoplasm to the lumen. As the pH drops, the high pK_a sites begin to leak protons, and then eventually stop participating in transport. This effectively lowers the number of protons transported to ATPs consumed per revolution; e.g., the coupling ratio. Lowering the coupling ratio makes it possible to achieve very acidic lumenal pHs. See Table SI for a list of parameters.

TABLE S I

V-ATPase Model Parameters

Parameter	Fig. 2 A	Fig. S3
Screening length ($1/\lambda$)	0.67 nm	0.67 nm
Rotational diffusion constant of rotor (D_r)	$10^4\ s^{-1}$	$10^4\ s^{-1}$
Proton diffusion constant (D_p)	$9.3 \times 10^9\ nm^2\ s^{-1}$	$9.3 \times 10^9\ nm^2\ s^{-1}$
Dielectric constant of cytoplasm (ϵ_c)	80	80
Dielectric constant of stator (ϵ_s)	4.0	4.0
Proton conductivity of lumenal channel	$2.2 \times 10^{10}\ M^{-1}\ s^{-1}$	$2.2 \times 10^{10}\ M^{-1}\ s^{-1}$
Proton conductivity of cytoplasmic channel	$2.2 \times 10^{10}\ M^{-1}\ s^{-1}$	$2.2 \times 10^{10}\ M^{-1}\ s^{-1}$
Radius of rotor (R)	3 nm	3 nm
Bilayer viscosity (η)	10 poise	10 poise
Zero load rotation rate of V_1	20 Hz	20 Hz
Free energy of ATP hydrolysis (ΔG_{ATP})	21 k_BT	21 k_BT
Central stator charge (elementary charge)	1.4	0.14
Rotor pK_a	5.4	8.1, 5.65
Radial position of central stator charge	3.54 nm	3.54 nm
Dipole length of protonated site	0.22 nm	0.16 nm, 0.39 nm
Cytoplasmic pH (pH_C)	See caption	7.4
Width of polar strip	0.79 nm	0.90 nm
Width of acidic channel	1.18 nm	1.43 nm
Width of hydrophobic interface	1.18 nm	2.5 nm

Parameters used in creating the V-ATPase pumping profile in Fig. 2 A (text) and the pumping curve in Fig. S3. In the right column, multiple entries refer to the value for the high and low rotor pK site, respectively.

Na-K ATPase Model

We have attempted to construct a more general model of the Na-K-ATPase pumping rate over a large range of environmental conditions. This was accomplished by simulating the detailed reaction schemes devised by Heyse et al. (1994) and Sokolov et al. (1998) while constraining the current to obey the voltage dependence measured by Sagar and Rakowski (1994). The model presented here is an amalgam of the most recent Apell model (Heyse et al., 1994), which focuses on sodium transport, with an older model that includes potassium transport. The kinetic scheme can be found in Fig. S4 A. The primary pumping cycle of this model, indicated by solid lines, closely resembles the standard Post-Albers scheme (Heyse et al., 1994). In addition, there are three escapements that involve incomplete pumping cycles. These closed loops are represented by dashed lines and are essential for describing the pump's behavior under extreme conditions such as low extracellular potassium concentrations.

Steady state values were computed by constructing the kinetic equations corresponding to the reaction scheme in Fig. S4 A and simulating their time evolution until steady state was reached. Alternatively, setting these equations equal to zero results in a set of linear coupled equations that can be solved algebraically to find the steady state values. For ease of implementation, we chose the former. The rate of ion transport was determined in the usual way by summing the forward and backward jump rates between those states that correspond to ion movement from the enzyme to the bulk cytoplasm (or the extracellular space).

To accurately describe pumping under physiological conditions, model parameters have been varied to obtain best fits to the current–voltage data measured by Sagar and Rakowski (1994). Four reverse rates along the potassium portion of the reaction cycle have been adjusted. Additionally, the reverse rates of four more parameters were modified to ensure detailed balance around each of the independent pump cycles. These parameters are indicated in Table SII (bold). To simulate the data from Sagar and Rakowski (1994), additional assumptions about cytoplasmic concentrations and the free energy of ATP must be made. For all simulations, the cytoplasmic values for ATP, ADP, and P_i can be found in Table I of the main article text. Sodium and potassium values can be found in Fig. S4.

Given an initial set of model parameters, the steady state current as a function of membrane potential was computed for each of the extracellular potassium concentrations examined by Sagar and Rakowski (1994). For each potassium concentration, the membrane potential was discretized and the reaction scheme simulated to determine the steady state current. This family of curves was then scaled by a common parameter to find the best simultaneous fit to all of the experimental data. Such a scale factor is required to normalize the single pump current to the experimentally measured current, which is the result of many pumps. This root mean square fitness score was then re-

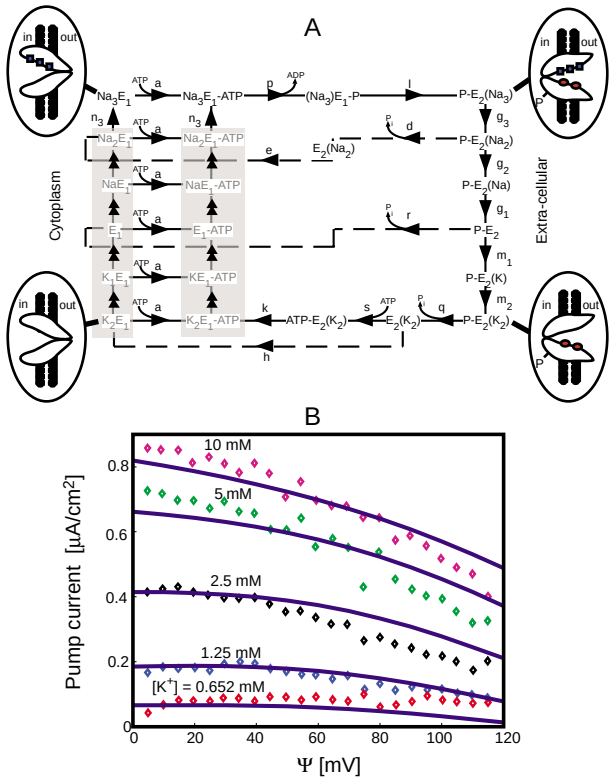

FIGURE S4. Na-K-ATPase reaction scheme and current voltage fit. (A) This reaction scheme combines aspects of two previous models published by Heyse et al. (1994) and Sokolov et al. (1998). The basic tenants of this model follow the accepted Post-Albers description that involves the pump switching between an inward and outward facing conformation, E_1 and E_2. Four cartoon diagrams have been included to illustrate the physical state of the enzyme. Chemical states within grayed regions are assumed to interconvert on a very fast time scale and are mathematically treated as one state. Please refer to the original papers for details concerning the construction of the differential equations from this reaction scheme. (B) The kinetic scheme in A is simulated using the model parameters in Table SII. The total number of pumps giving rise to the measured current is unknown; thus, an arbitrary scale factor has been used to scale the single pump current (solid line) to the experimentally measured data (◇). Cytoplasmic sodium and potassium concentrations are held constant at 20 and 120 mM, respectively. Lumenal sodium concentration is initially 120 mM. Data is adapted from Figure 5 A of Sagar and Rakowski (1994).

TABLE SII

Na-K-ATPase Model Parameters

Parameter	Forward value/ equilibrium constant	Reverse value	Dielectric coefficient	
n_3	$2 \times 10^4\ M^{-1}\ s^{-1}$	$80\ s^{-1}$	$\alpha = 0.25$	Sokolov et al. (1998)
a	$3.5 \times 10^6\ M^{-1}\ s^{-1}$	$2.76 \times 10^{-1}\ s^{-1}$*	0	Sokolov et al. (1998)
p	$600\ s^{-1}$	$1.5 \times 10^6\ M^{-1}\ s^{-1}$	0	Sokolov et al. (1998)
l	$25\ s^{-1}$	$2.75\ s^{-1}$	$\beta = 0.1$	Sokolov et al. (1998)
g_3	$1.4 \times 10^3\ s^{-1}$	$1.4 \times 10^4\ M^{-1}\ s^{-1}$	$\delta_0 = 0.65$	Sokolov et al. (1998)
g_2	$5 \times 10^3\ s^{-1}$	$3.25 \times 10^3\ M^{-1}\ s^{-1}$	$\delta_1 = 0.1$	Sokolov et al. (1998)
g_1	$7 \times 10^2\ s^{-1}$	$7.77 \times 10^3\ M^{-1}\ s^{-1}$	$\delta_2 = 0.1$	Sokolov et al. (1998)
r	$0.023\ s^{-1}$	$3.10 \times 10^3\ M^{-1}\ s^{-1}$*	$\gamma = 1.8$	Sokolov et al. (1998)
d	$1.4\ s^{-1}$	$2.45\ M^{-1}\ s^{-1}$*	0	Sokolov et al. (1998)
e	$50\ s^{-1}$	$2.5 \times 10^2\ s^{-1}$	0	Sokolov et al. (1998)
k	$22\ s^{-1}$	$8.71\ s^{-1}$*	0	Heyse et al. (1994)
h	$0.1\ s^{-1}$	$10^2\ s^{-1}$	0	Heyse et al. (1994)
s	$5 \times 10^5\ M^{-1}\ s^{-1}$	$9.95 \times 10\ s^{-1}$*	0	Heyse et al. (1994)
q	$10^5\ s^{-1}$	$7.58 \times 10^5\ M^{-1}\ s^{-1}$*	0	Heyse et al. (1994)
m_1	$3.4 \times 10^4\ M^{-1}\ s^{-1}$	$1.14 \times 10^2\ s^{-1}$*	$\epsilon_1 = 0.1$	Heyse et al. (1994)
$\mathbf{m_2}$	$5 \times 10^6\ M^{-1}\ s^{-1}$	$3.83 \times 10^6\ s^{-1}$*	$\epsilon_2 = 0.1$	Heyse et al. (1994)
K_{Na}	3×10^{-3} M	—	0	Sokolov et al. (1998)
K_K	1.2×10^{-2} M	—	0	Heyse et al. (1994)

Parameters used for the Na-K-ATPase pumping profile. *Parameters differ from the values presented in the references. The kinetic scheme presented in Fig. S4 A has four closed loops. Detailed balance has been enforced around each of these loops by constraining the reverse rates of the parameters set off in bold. The remaining four * parameters correspond to reverse rates along the potassium pumping portion of the cycle. These parameters have been determined from fitting current voltage data (Fig. S4 B).

corded. A Nelder-Mead algorithm was used to search through the space of model parameters and find the set that minimized the fitness score (Press, 1997). These parameters are presented in Table SII, and the fit to the data is presented in Figure S4 B. In all figures, ionic flux from the cytoplasm to the extra-cellular/lumenal space is defined to be positive, and the membrane potential is defined relative to the lumen. Thus, a positive membrane potential will induce positive charges to flow in the negative direction.

This calibrated model has been used to compute the sodium and potassium rates over a wide range of external/lumenal concentrations and membrane potentials. To illustrate what a slice of this surface looks like, the sodium rate is plotted as a function of membrane potential and lumenal potassium concentration in Figure 2B. It is this response surface combined with the corresponding surface for the potassium flux that are used to simulate the effect of incorporating Na-K-ATPases in model vesicles. When creating these surfaces, cytoplasmic concentrations of all species are assumed constant. Values can be found in Table I of the main article text.

These computations are given in program files: nak_pump.m (main program); delta.m; nak_param.m.

Buffering Capacity

When a proton enters the lumen or the cytoplasm, it will equilibrate with the lumenal matrix. A bound proton is then no longer free to contribute to the pH in that compartment. The ability of the matrix to bind free protons is referred to as its buffering power. The standard definition of buffering power originally given by Michaelis is (Roos and Boron, 1981):

$$\beta = \frac{\Delta[B]}{\Delta pH}, \tag{1}$$

where $\Delta[B]$ is the amount of strong base added to the system. Since $\Delta[B] \cong \Delta[H^+]$, the relation between change in pH and change in proton concentration is determined. Some experiments suggest that the buffering capacity of some organelles is nearly constant in the pH range 6–8 (Farinas and Verkman, 1999; Wu et al., 2000). However, Van Dyke and Belcher (1994) find that the buffering capacity of endosomes depends strongly upon the lumenal pH (Fig. S5).

In the simplest case, there is only one kind of proton accepting site with some intrinsic pK_a. Once the internal pH goes below this pK_a, the buffering ability of the matrix quickly diminishes. From the definition of pH, one then obtains a buffering capacity, $\beta \propto 10^{-pH}$. In reality, the matrix is composed of many titratable sites with a distribution of pK_a's. With this interpretation, the jagged variation in the buffer capacity found by Van Dyke and Belcher (1994) seems more reasonable.

A sensitivity analysis shows that the buffering capacity is one of the most dominant factors in determining the shape of the acidification curves. Originally, it was our goal to try to recreate the pumping performance of the V-ATPase from the experimentally measured curves in Figs. 3 and 4 (text). This would serve as a calibration for the proton pump. However, uncertainties in the volume and buffering capacity made it impossible to extract dependable information about the pump.

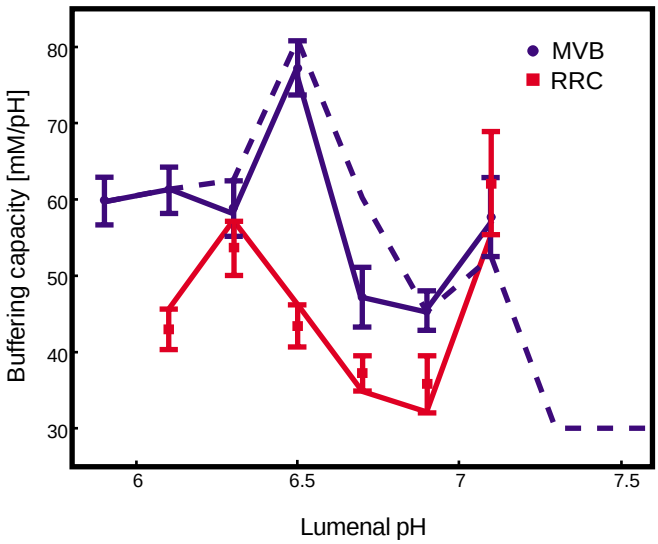

FIGURE S5. Endosomal buffering capacity as a function of pH. The buffering capacities of RRC (■) and MVB (●) vesicles have a strong dependence on lumenal pH (data reproduced from Van Dyke and Belcher, 1994). For each of the two vesicle populations, the true buffering curve was approximated by a linear interpolation of the buffering data (solid lines). These curves were used to simulate the acidification of the respective vesicle populations in Fig. 4 (text). In addition, the effect on acidification of a constant versus nonconstant buffering curve (dashed line) is explored in Fig. 3, A and B (text).

Surface Potentials

Here we address how our description of pH regulation is affected by negatively charged lipids on the cytoplasmic leaflet of organelles. First consider an organelle permeable to ions, but with no surface charge or pumps. At equilibrium, only a Donnan potential, $\Delta\psi$, will exist across the organelle due to the impermeable macro-ions. If a negative surface potential is imposed on the organelle, $-\Delta\phi$, the surface values of positive (negative) ions in solution will increase (decrease) by a Boltzmann factor (see Eq. 4 in text). The concomitant flow of ions quickly builds up an opposing membrane potential, $\Delta\psi \rightarrow \Delta\psi + \Delta\phi$. Changes in lumenal concentrations are marginal since very few ions are required to produce a sizable membrane potential. Thus, the addition of a surface potential shifts the balance of the (equilibrium) electrochemical potential from a chemical to an electrical gradient, while the magnitude remains unchanged. However, steady state and transient dynamics do depend upon surface potentials since channel and pump activities depend on the relative magnitudes of the concentration and electrical components of the electrochemical potential.

Consider the determination of Golgi proton permeability in Fig. 6, inset (text). In the absence of surface charge, membrane potentials are very small and an analytic analysis is possible. To see how this simulation depends on surface potential, we must consider our model for proton flux:

$$J_{\phi=0} = P \cdot S \cdot U \cdot \frac{([H^+]_L - [H^+]_C \cdot e^{-U})}{1 - e^{-U}} \approx P \cdot S \cdot ([H^+]_L - [H^+]_C \cdot e^{-U}). \tag{2}$$

When the reduced surface potential, $-\Delta\Phi$, is added $[H^+]_C \rightarrow [H^+]_C \cdot \exp(+\Delta\Phi)$ and $U \rightarrow U + \Delta\Phi$, as discussed above. Because of the exponential Boltzmann factor, the membrane potential is no longer negligible. The proton flux is:

$$\begin{aligned} J_{\Delta\phi\neq 0} &= P \cdot S \cdot (U + \Delta\Phi) \cdot \frac{\{[H^+]_L - [H^+]_C \cdot e^{-(U+\Delta\Phi)}\}}{1 - e^{-(U+\Delta\Phi)}} \\ &\approx P \cdot S \cdot \Delta\Phi \cdot \frac{([H^+]_L - [H^+]_C \cdot e^{-U})}{1 - e^{-\Delta\Phi}} \\ &= J_{\Delta\phi=0} \cdot \left(\frac{\Delta\Phi}{1 - e^{-\Delta\Phi}}\right), \end{aligned} \tag{3}$$

where the approximation $U + \Delta\Phi \sim \Delta\Phi$ has been made. When $\Delta\phi = -50$ mV, the cofactor in the last equation $\approx$2.27. When the simulation is rerun without the surface potential, the best fit permeability is exactly 2.27× larger than the one reported in Table IV (main article text).

From this example, we see that proton fluxes can be two to three times smaller in the absence of surface charge. This makes the pH simulations in Figs. 3 and 4 (text) undershoot the present trajectories by ~0.2–0.3 pH units, if the proton pump remains unaffected by the changes in membrane potential and surface concentrations. However, in our model for the proton pump, the rate-limiting step near cytoplasmic pH values is the capture of a proton from the cytoplasm. Removal of the −50-mV surface potential lowers the surface concentration of protons by a factor of 10. This decreases the pumping rate by ~1.7× when the lumen is near neutral pH. Examination of the sodium performance surface (Fig. 2 B, text) in the absence of a surface potential reveals a less dramatic influence on the dynamics (<6 Na^+/s). Thus, only the exact pump numbers and permeability values change in the absence of surface potentials, and the nature of our presentation is unaffected.

REFERENCES

Alberts, B., D. Bray, J. Lewis, M. Raff, K. Roberts, and J. Watson. 1994. Molecular Biology of the Cell. 3rd ed. Garland Press, New York, NY. 1294 pp.

Boekema, E., T. Ubbink-Kok, J. Lolkema, A. Brisson, and W. Konings. 1997. Visualization of a peripheral stalk in V-type ATPase: evidence for the stator structure essential to rotational catalysis. *Proc. Natl. Acad. Sci. USA*. 94:14291–14293.

Dimroth, P., H. Wang, M. Grabe, and G. Oster. 1999. Energy transduction in the sodium F-ATPase of Propionigenium modestum. *Proc. Natl. Acad. Sci. USA*. 96:4924–4929.

Eisenberg, E., and T. Hill. 1985. Muscle contraction and free energy transduction in biological systems. *Science*. 227:999–1006.

Elston, T., H. Wang, and G. Oster. 1998. Energy transduction in ATP synthase. *Nature*. 391:510–514.

Farinas, J., and A.S. Verkman. 1999. Receptor-mediated targeting of fluorescent probes in living cells. *J. Biol. Chem*. 274:7603–7606.

Finbow, M., and M. Harrison. 1997. The vacuolar H^+-ATPase: a universal proton pump of eukaryotes. *Biochem. J*. 324:697–712.

Forgac, M. 1999. Structure and properties of the vacuolar (H^+)-ATPases. *J. Biol. Chem*. 274:12951–12954.

Forgac, M. 2000. Structure, mechanism and regulation of the clathrin-coated vesicle and yeast vacuolar H^+-ATPases. *J. Exp. Biol*. 203:71–80.

Grabe, M., H. Wang, and G. Oster. 2000. The mechanochemistry of V-ATPase proton pumps. *Biophys. J.* 78:2798–2813.
Heyse, S., I. Wuddel, H.-J. Apell, and W. Stuermer. 1994. Partial reactions of the Na,K-ATPase: determination of rate constants. *J. Gen. Physiol.* 104:197–240.
Junge, W., H. Lill, and S. Engelbrecht. 1997. ATP synthase: an electro-chemical transducer with rotatory mechanics. *Trends Biochem. Sci.* 22: 420–423.
Murata, T., K. Igarashi, Y. Kakinuma, and I. Yamato. 2000. Na^+ binding of V-type Na^+-ATPase in *Enterococcus hirae*. *J. Biol. Chem.* 275:13415–13419.
Press, W.H. 1997. Numerical Recipes in C: The Art of Scientific Computing. 2nd ed. Cambridge University Press, New York, NY. 994 pp.
Roos, A., and W.F. Boron. 1981. Intracellular pH. *Physiol. Rev.* 61:296–434.
Sagar, A., and R.F. Rakowski. 1994. Access channel model for the voltage dependence of the forward-running Na^+/K^+ pump. *J. Gen. Physiol.* 103:869–894.
Sokolov, V.S., H.-J. Apell, J.E.T. Corrie, and D.R. Trentham. 1998. Fast transient currents in Na,K-ATPase induced by ATP concentration jumps from the P3-(1-(3′,5′-dimethoxyphenyl)-2-phenyl-2-oxo)ethyl ester of ATP. *Biophys. J.* 74:2285–2298.
Van Dyke, R.W., and J.D. Belcher. 1994. Acidification of three types of liver endocytic vesicles: similarities and differences. *Am. J. Physiol.* 266: C81–C94.
Vik, S.B., and B.J. Antonio. 1994. A mechanism of proton translocation by F1F0 ATP synthases suggested by double mutants of the a subunit. *J. Biol. Chem.* 269:30364–30369.
Wu, M., J. Llopis, S. Adams, J. McCaffery, T. Machen, H.P. Moore, and R. Tsien. 2000. Using targeted avidin and membrane permeant fluorescent biotin to study secretory pathway organelle pH regulation. *Chem. Biol.* 7:197–209.